Research Article

ADVANCED PHOTONICS

High performance and stable pure-blue quasi-2D perovskite light-emitting diodes by multifunctional zwitterionic passivation engineering

Chao Shen,[a,b,†] Shuyan Fang,[a,†] Jibin Zhang,[c,*] Xiangfei Liang,[a] Chenhui Su,[a] Jian Qing,[a] Wanzhu Cai,[a] Yunhan Luo,[b,d,*] Renqiang Yang,[e] and Lintao Hou[a,*]

[a]Jinan University, College of Physics and Optical Engineering, Guangdong Provincial Engineering Technology Research Center of Vacuum Coating Technologies and New Energy Materials, Guangzhou Key Laboratory of Vacuum Coating Technologies and New Energy Materials, Guangzhou, China
[b]Jinan University, College of Physics and Optical Engineering, Guangdong Provincial Key Laboratory of Optical Fiber Sensing and Communications, Guangzhou, China
[c]Zhengzhou University, School of Physics and Microelectronics, Key Laboratory of Materials Physics of Ministry of Education, Zhengzhou, China
[d]Jinan University, Key Laboratory of Optoelectronic Information and Sensing Technologies of Guangdong Higher Education Institutes, Guangzhou, China
[e]Jianghan University, School of Optoelectronic Materials and Technology, Key Laboratory of Optoelectronic Chemical Materials and Devices of Ministry of Education, Wuhan, China

Abstract. Despite the rapid advances of red and green perovskite light-emitting diodes (PeLEDs), achieving high brightness with high external quantum efficiency (EQE) remains a challenge for the pure-blue PeLEDs, which greatly hinders their practical applications, such as white-light illumination and in optical communication as a high-speed and low-loss light source. Herein, we report a high-performance pure-blue PeLED based on mixed-halide quasi-2D perovskites incorporated with a zwitterionic molecule of 3-(benzyldimethylammonio) propanesulfonate (3-BAS). Experimental and density functional theory analysis reveals that 3-BAS can simultaneously eliminate non-radiative recombination loss, suppress halide migration, and regulate phase distribution for smoothing energy transfer in the mixed-halide quasi-2D perovskites, leading to the final perovskites with high photoluminescence quantum yield and robust spectrum stability. Thus, the high-performance pure-blue PeLED with a recorded brightness with 1806 cd m^{-2} and a relative higher EQE of 9.25% is achieved, which is successfully demonstrated in a visible light communication system for voice signal transmission. We pave the way for achieving highly efficient pure-blue PeLEDs with great application potential in future optical communication networks.

Keywords: pure-blue PeLEDs; quasi-2D perovskite; zwitterionic additive; visible light communication.

Received Nov. 15, 2023; revised manuscript received Jan. 10, 2024; accepted for publication Feb. 2, 2024; published online Feb. 26, 2024.

[DOI: 10.1117/1.AP.6.2.026002]

1 Introduction

Metal halide perovskite light-emitting diodes (PeLEDs) have emerged as prospective candidates for high-resolution display and communication applications because of their tunable bandgaps, high photoluminescence quantum yields (PLQYs), and good color purity.[1–5] Since the first report of PeLEDs by Tan et al. in 2014,[6] external quantum efficiencies (EQEs) exceeding 20% have been achieved at red and near-infrared wavelengths,[7–9] and the state-of-the-art green PeLEDs exhibit outstanding EQEs of over 30%.[10] To date, the EQEs of sky-blue perovskites (480 to 500 nm)-based PeLEDs have exceeded 16%;[11] however, as one

*Address all correspondence to Jibin Zhang, jbzhang@zzu.edu.cn; Yunhan Luo, yunhanluo@163.com; Lintao Hou, thlt@jnu.edu.cn

†These authors contributed equally to this work.

of primary colors, the efficiency and brightness of pure-blue PeLEDs (460 to 470 nm) are still largely lagging behind. Although the EQE of the pure-blue electroluminescent device is over 11%, its brightness is as low as 1000 cd m^{-2}, which severely restricts the development for illumination and display applications (≥1000 cd m^{-2}).[12] Therefore, it is urgent to develop new strategies to further promote the performance of pure-blue PeLEDs.

Mixed-halide chloride/bromide (Cl/Br) quasi-2D perovskites afford an efficient approach for pure-blue PeLEDs through a simple solution preparation process.[13–16] The general formula of mixed-halide pure-blue emission perovskites is $L_2A_{n-1}Pb_n(Cl/Br)_{3n+1}$, where A is a monovalent cation, such as Cs^+, methylammonium (MA^+), or formamidinium (FA^+); L is a large-sized organic spacer cation, such as butylammonium (BA), phenylethylammonium (PEA), or naphthylmethylamine; n represents the number of lead halide octahedral ($[Pb(Cl/Br)_6]^{4-}$) layers sandwiched between the organic spacers. The nanosheets of $[Pb(Cl/Br)_6]^{4-}$ are separated by the organic spacer cation, and various quantum wells with different n-values will be formed.[17,18] There are three key points that determine the performance of the pure-blue quasi-2D PeLEDs. First, the small-n phases (especially for $n = 1$) in quasi-2D perovskites have been demonstrated to cause inefficient energy transfer because of their strong excitonic phonon coupling.[19,20] Second, massive undercoordinated Pb^{2+} related halide vacancies at the surface of the perovskite crystals result in a high density of deep-level defects and large nonradiative recombinations.[21,22] Moreover, halide migration in the mixed-halide perovskites is usually accelerated under an electric field because of the weak van der Waals forces between monovalent cations and halides of the $[Pb(Cl/Br)_6]^{4-}$ octahedron, leading to serious electroluminescence (EL) spectral shift and device performance degradation.[23,24] Taking these issues into account, optimizing the perovskite phase distribution, passivating undercoordinated Pb^{2+} related defects, and suppressing halide migration in mixed-halide Cl/Br based quasi-2D perovskites are of paramount importance in creating highly efficient and luminescent deep-blue PeLEDs.

Here, we propose a multifunctional zwitterionic molecule of 3-(benzyldimethylammonio) propanesulfonate (3-BAS) to promote the photoelectric properties and phase stability of the mixed-halide quasi-2D pure-blue PeLEDs. Theoretical and experimental investigations reveal that the sulfonic group ($-SO_3^-$) of 3-BAS can interact with the uncoordinated Pb^{2+} through Lewis base-acid reaction for passivating the surface defects of the quasi-2D perovskites. In addition, the electropositively quaternary ammonium group ($-R_4N^+$) of 3-BAS can interact with the electronegatively halide ions of the perovskites via the formation of electrostatic interactions, thus suppressing the migration of halides. More importantly, the crystallization kinetics of quasi-2D perovskites can be regulated by a 3-BAS molecule, leading to a decreased ratio of small-n phase with smoothing energy transfer pathway in mixed quasi-2D perovskites. Based on the optimized perovskites emitter, pure-blue PeLEDs emitting at 466 nm are achieved with a record luminance of 1806 cd m^{-2}, EQE of nearly 10%, and a negligible EL shift under different electrical bias, identifying one of the best performing candidates among pure-blue quasi-2D PeLEDs reported in the literature so far. What is more, the advantageous features of 3-BAS-treated pure-blue PeLEDs, including short response time, high brightness, and stable EL spectra, perfectly match the strict requirements of the light sources for next-generation ultrahigh-speed visible light communication (VLC).

2 Results and Discussion

To give a first glance of the intermolecular interaction between perovskites and 3-BAS, we adopt density functional theory (DFT) calculations to analyze the relationship among theoretically associated variables. The chemical structure and simulated electrostatic potential (ESP) of the 3-BAS molecule are shown in Fig. 1(a). It is clear that the negative charge (lone electron pairs) of 3-BAS is mainly delocalized on oxygen atoms of the $-SO_3^-$ group (light red color). As the electron-rich group tends to coordinate with uncoordinated Pb^{2+} ions in perovskites through the Lewis base-acid reaction,[25,26] the $-SO_3^-$ group of 3-BAS can perfectly coordinate with the uncoordinated Pb^{2+} cations through the formation of Lewis adducts, which provides an efficient way to passivate the trap defects at surface of the perovskites. In contrast, the electron-deficient group of $-R_4N^+$ shows positive charge (light blue color), which means that the electrostatic interactions can be easily formed between $-R_4N^+$ and negatively uncoordinated halide ions of the perovskites.[27–29] Thus, we speculate that the 3-BAS molecule can interact with the perovskites via synergetic effects from both Lewis base-acid and electrostatic interactions, which might remarkably minimize the number of undercoordinated Pb^{2+} and halide-related trap defects and thus improve the stability of mixed-halide quasi-2D perovskites. The vacancy formation energies of perovskites with (w/) and without (w/o) the 3-BAS passivation are determined through a simplified model of 3-BAS/$CsPbBr_3$, and the surface configuration after relaxation is given in Fig. S1 in the Supplementary Material. The vacancy formation energy of the perovskites exhibits great improvement of ∼0.7 eV after 3-BAS passivation [Fig. 1(b)], suggesting that 3-BAS can prevent the loss of surface halide atoms, which is essential for the formation of perfect $[PbX_6]^{4-}$ octahedra and the decrease of the small-n phase during the crystallization process of the perovskites.

To further understand the defect passivation by incorporating 3-BAS, we conducted projected density of states (PDOS) calculations of the structural configuration of perovskites w/ and w/o 3-BAS. The perovskites with undercoordinated Pb^{2+} feature conspicuous trap states [Fig. 1(c)], which can capture excited carriers and result in severe nonradiative recombinations with decreased PLQYs.[30,31] In contrast, the trap states of the perovskites reduce distinctly after being passivated by 3-BAS [Fig. 1(d)], suggesting that 3-BAS possesses a good capability to improve the optoelectronic performance of perovskites. Figure 1(e) shows the differential charge density plot of the 3-BAS/$CsPbBr_3$ system. It can be found that the $-SO_3^-$ group is close to the uncoordinated Pb^{2+} cation through forming a Pb-O coordinate bond, and the interface charge redistributions on the $-SO_3^-$ group and $-R_4N^+$ group confirm the formation of Lewis base-acid reaction and electrostatic interactions between 3-BAS and perovskites.[32] In addition, the delocalized π-electrons on the benzene ring of 3-BAS are beneficial to the charge transfer between individual perovskite crystals, which is imperative for enhancing the performance of photoelectric devices.[33]

The Cl-Br mixed quasi-2D perovskites thin films were deposited onto indium tin oxide (ITO)/poly(9-vinylcarbazole) (PVK) substrates using a one-step spin-coating method; the details about the film fabrication and precursor recipes are presented in the Supplementary Material. The perovskites with the

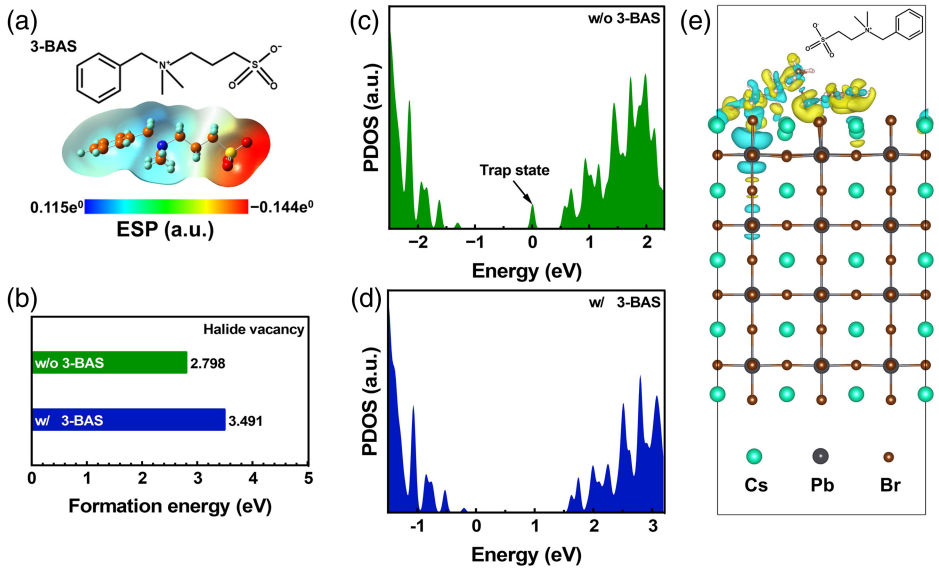

Fig. 1 (a) Chemical structure and simulated ESP of 3-BAS molecule. (b) Vacancies formation energies of halide for the perovskites before and after 3-BAS passivation. Calculated PDOS of the perovskites (c) w/o and (d) w/ 3-BAS molecule passivation based on a simplified model. (e) Differential charge density plot of the 3-BAS/perovskite system (isosurface value of 0.0015 e/Å). In the three-dimensional plot, the yellow and green regions of charge density denote the charge accumulation and depletion, respectively.

pure-blue emission at 466 nm can be obtained when the ratio of bromide and chloride is 2:1, as shown in Fig. S2 in the Supplementary Material. To further confirm the chemical interactions between 3-BAS and perovskites, we performed Fourier transform infrared (FT-IR) measurement to analyze the S=O stretching vibration ν (S=O) of the $-SO_3^-$ group and C-N stretching vibration ν (C-N) of the $-R_4N^+$ group for neat 3-BAS and 3-BAS + $PbBr_2$ composites. It can be seen that the ν (S=O) of neat BAS at ~1041 cm^{-1} shifts to a lower wavenumber (~1034 cm^{-1}) for the 3-BAS + $PbBr_2$ composites [Fig. 2(a)], indicating the coordination of the $-SO_3^-$ group and undercoordinated Pb^{2+} cations. Meanwhile, the peak at ~736 cm^{-1} derived from the ν (C-N) for the positively charged $-R_4N^+$ group of neat 3-BAS shifts to a lower wavenumber of ~727 cm^{-1} in the presence of $PbBr_2$ [Fig. 2(b)], suggesting the formation of noncovalent electrostatic interactions between the positively charged $-R_4N^+$ group of 3-BAS and the negatively charged halides. Furthermore, X-ray photoelectron spectroscopy (XPS) measurements were carried out to verify the synergistic effect of both the Lewis base-acid reaction and electrostatic interactions formation. In Fig. 2(c), the peaks at 166.5 and 168.4 eV in the targeted perovskite film can be assigned to S $2p_{3/2}$ and S $2p_{1/2}$, respectively, indicating the presence of 3-BAS in targeted perovskites compared to the control film. Figure 2(d) shows the XPS spectra of Pb 4f, where both Pb $4f_{7/2}$ (136.9 eV) and Pb $4f_{5/2}$ (141.8 eV) peaks shift to lower binding energy with the incorporation of 3-BAS. Such negative shifts of Pb 4f binding energy can be ascribed to the increased electron cloud density around Pb^{2+} cations, as explained by the fact that the $-SO_3^-$ donates its lone electron pair to the empty 6p orbital of Pb^{2+} by forming Lewis adducts.[34] Meanwhile, negative shifts are also observed in both Br 3d and Cl 2p spectra [Figs. 2(e) and 2(f)], suggesting that Lewis base groups donate electrons to Pb^{2+} (which reduces their positive charge); thereby the interaction between Pb^{2+} and halogen ions is altered,[20] which is in accordance with the DFT calculation results. Based on the above analysis, we can conclude that the 3-BAS molecule can effectively interact with the quasi-2D perovskites via synergetic effects of both electrostatic interaction formation and the Lewis base-acid reaction, which will remarkably enhance phase stability and minimize nonradiative recombination loss in the quasi-2D perovskites.

To modulate the photoelectric properties of the pure-blue perovskite film, the 3-BAS molecule was incorporated with an optimized 3-BAS/Pb^{2+} concentration of 10% (volume fraction). The 3-BAS-processed perovskite film shows the highest PL intensity, with PLQY increased by 100% when compared to the control sample [Fig. 3(a) and Fig. S3 in the Supplementary Material]. The average PL lifetime (τ_{avg}) of the control perovskite film is 13.61 ns, while the targeted perovskite film exhibits a much longer τ_{avg} of 27.88 ns (Fig. S4 and Table S1 in the Supplementary Material), revealing the reduced trap-related nonradiative recombinations in the optimized sample.[35] We further fabricated the hole-only device with the structure of ITO/PVK/PVP/perovskites/MoO_x/Ag to quantify the trap density with the assistance of a space charge-limited current technique (Fig. S5 in the Supplementary Material), which can be achieved by the following equation:[21]

$$N_t = \frac{2\varepsilon_0\varepsilon_r V_{\mathrm{TFL}}}{qL^2},$$

where ε_r and ε_0 are the relative dielectric constant and vacuum permittivity, L is the thickness of the perovskite film, q is a single charge, and V_{TFL} is the trap-filling limit voltage that can be determined from the current density–voltage curve. The trap densities of the perovskite films are reduced by 43% from 3.43×10^{17} to 2.40×10^{17} cm^{-3} after incorporation of the

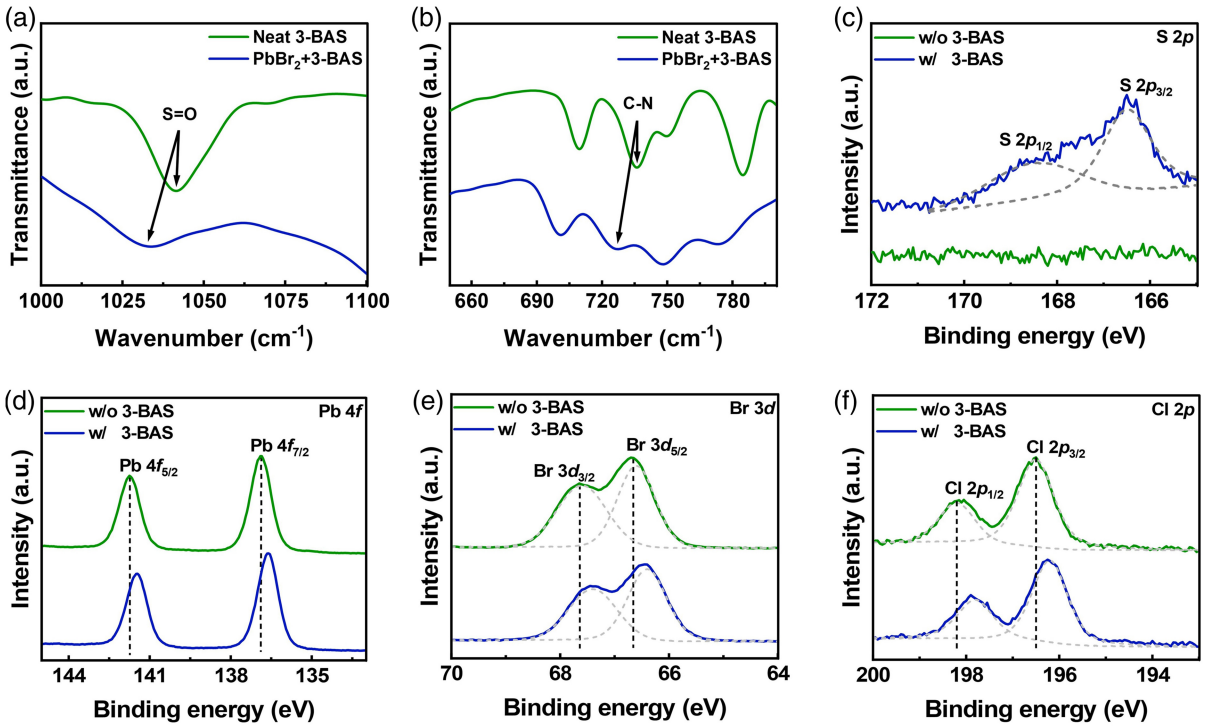

Fig. 2 (a), (b) FT-IR spectra of S=O and C-N vibration modes of 3-BAS and 3-BAS-incorporated $PbBr_2$. High-resolution XPS spectra of (c) S 2p, (d) Pb 4f, (e) Br 3d, and (f) Cl 2p for the control and targeted perovskite films.

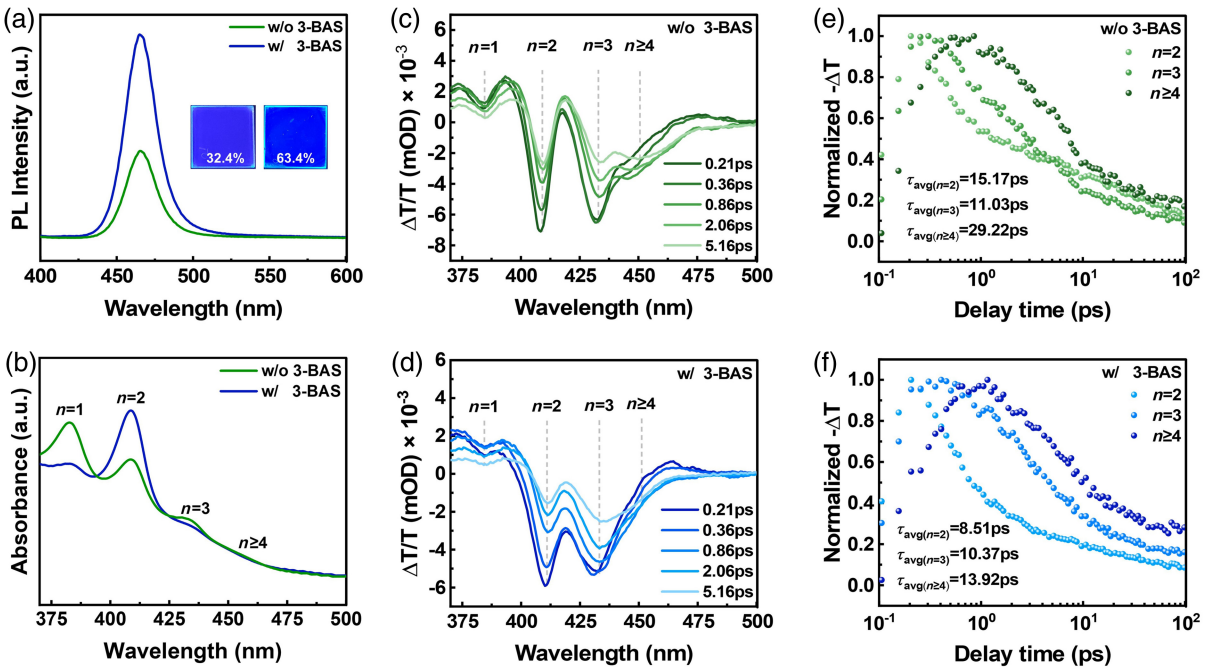

Fig. 3 (a) PL and (b) UV-vis absorption spectra of the pure-blue quasi-2D control and targeted perovskite films. (c), (d) TA spectra of the quasi-2D control and targeted perovskite films with evolution time from 0.21 to 5.16 ps. (e), (f) TA kinetics probed at selected wavelengths for the pure-blue quasi-2D control and targeted perovskite films.

3-BAS molecule, which can eliminate the unwanted nonradiative recombination to a certain extent. To verify the influence of 3-BAS on the structure stability of perovskites, we then monitored peak positions and intensities of PL spectra of the perovskite films w/ and w/o 3-BAS in the atmosphere with constant relative humidity of 40% and room temperature of 25°C. As shown in Fig. S6 in the Supplementary Material, the PL intensity of the control perovskite film suffers a severe decline with a large peak redshift, from 466 to 482 nm. On the contrary, the targeted perovskite film shows negligible variation in both PL peak position and intensity, indicating that the incorporation of the 3-BAS molecule is very important for reducing defect formation and improving the structure stability of the Cl-Br mixed quasi-2D perovskites. In addition, we also conducted temperature- and UV light-dependent stability tests for the control and targeted perovskite films. As shown in Figs. S7(a) and S7(b) in the Supplementary Material, the targeted film exhibits much better thermal stability compared to the control one. Similar results were also obtained under a continuous UV light exposure condition [Figs. S7(c) and S7(d) in the Supplementary Material]. To explore the origin of increased film moisture stability, the water contact angles of the control and targeted perovskite films were measured, as shown in Fig. S8 in the Supplementary Material. The contact angle of the control perovskite film was determined to be 27.4 deg, which was enhanced to 38.9 deg when incorporated with 3-BAS. This would be one of the reasons that the hydrophobic perovskite with 3-BAS exhibits improved moisture stability in air.[36]

To investigate the ion migration in perovskite, we conducted forward and reverse current–voltage scanning for both control and targeted devices. As shown in Figs. S9(a) and S9(b) in the Supplementary Material, significant hysteresis was observed within the first three scanning cycles for the control device, whereas the targeted device remained stable even after 30 cycles. Therefore, ion migration is effectively suppressed in the 3-BAS treated PeLED as current–voltage hysteresis is known to be associated with ion transport in perovskite devices.[25,37] Furthermore, we conducted microscopic PL imaging to support our findings. Specifically, we applied a constant bias (4.0 V) across the perovskite film between two in-plane Ag electrodes [Figs. S9(c) and S9(d) in the Supplementary Material]. For the control film, a noticeable decrease in PL intensity was observed at dark spots, which then gradually extended across the entire perovskite film. In contrast, no significant decrease in PL intensity was observed in the targeted device. All these results collectively indicate that 3-BAS can effectively suppress ion migration in perovskite materials.[37]

For investigating the phase distribution of the perovskite films before and after incorporation of 3-BAS molecule, we then conducted ultraviolet-visible spectroscopy (UV-vis) measurement. As shown in Fig. 3(b), the four UV-vis shoulder peaks at 383, 410, 435, and 460 nm can be assigned to $n = 1$, 2, 3, and 4 phases of the Cl-Br mixed quasi-2D perovskites, respectively. Compared with the control perovskite film, the absorbance intensities at ~383 and 435 nm related to $n = 1$ and $n = 3$ phases reduce significantly for the targeted perovskite film, suggesting that the perovskite phases are redistributed after incorporation of 3-BAS. We speculate the strong interaction of 3-BAS with Pb^{2+} and halide ions retards the crystallization kinetics of perovskite films, inhibiting the formation of $n = 1$ phase at the early stage of film growth. As a result, more $n = 2$ phase $[PbX_6]^{4-}$ octahedrons with the spacer cation of PEA^+ are easily formed because of the low formation energy. At the same time, the $n = 3$ phase was inhibited because of the consumption of a large number of PEA^+ in the formation of $n = 2$ phase.[20] Grazing-incidence wide-angle X-ray scattering patterns were further performed to investigate the effect of the 3-BAS on the perovskites' crystallization and orientation. As shown in Fig. S10 in the Supplementary Material, the control film exhibits a uniform (110) diffraction ring in the entire plane, originating from the large phase ($n \geq 4$). In contrast, too short (110) Bragg scattering arcs appear after incorporation of 3-BAS, suggesting the well-oriented distribution of perovskite layers ($n \geq 4$) for the targeted perovskite film.[38–40] Furthermore, the targeted perovskites film exhibits much weaker diffraction patterns at $q_{xy} = 0.36$ Å^{-1} and $q_{xy} = 0.92$ Å^{-1} (Fig. S11 in the Supplementary Material), indicating that 3-BAS can inhibit the formation of small-n phases during the perovskite crystallization. In addition, the strong interaction between 3-BAS and perovskites can also modulate the film morphology with better uniformity and lower surface roughness (Figs. S12 and S13 in the Supplementary Material), which is also beneficial to the improvement of the optoelectronic properties of devices.

Based on the previous analysis, reducing small-n phase (especially for $n = 1$) is vital for promoting energy transfer between quasi-2D perovskite layers toward high-performance PeLEDs.[39,41] We then performed ultrafast transient absorption (TA) spectroscopy to investigate the energy transfer dynamics for the control and targeted perovskite films. The pseudo-color TA spectrograms of the samples are presented in Fig. S14 in the Supplementary Material, in which the blue negative parts represent ground-state bleach with the peaks at 383, 410, 435, and 460 nm, corresponding well to $n = 1$, $n = 2$, $n = 3$, and $n \geq 4$ phases, respectively. The photogenerated carriers are primarily formed in small-n phases and then transfer to large-n phases when prolonging the decay time, suggesting that there is an efficient energy transfer process from small-n phases to high-n phases. Figures 3(c) and 3(d) show that the bleaching intensity of the $n = 1$ phase in the targeted perovskites is lower than that of the pristine sample, indicating that the small-n phase of the deep-blue quasi-2D perovskites is suppressed due to the optimized phase distribution after incorporation of the 3-BAS molecule. To further study the energy transfer process, the time traces of $n = 2$, $n = 3$, and $n \geq 4$ phases are extracted respectively, as shown in Figs. 3(e) and 3(f) and Table S2 in the Supplementary Material. According to the fitting parameters, the decay time of $n = 2$, $n = 3$, and $n \geq 4$ phases for the control perovskites is 15.17, 11.03, and 29.22 ps, respectively, which is longer than 8.51, 10.37, and 13.92 ps for the targeted perovskites, suggesting that carrier transformation process from small-n phase to large-n phase becomes highly efficient and fast in the targeted perovskite film with optimized phase distribution, further improving the PLQY by nearly 100%. As discussed above, both passivating undercoordinated Pb^{2+} related defects with suppressed halide ion migration and reducing small-n phase have jointly contributed to improving the luminescent performance of the targeted perovskite.

Based on the optimized pure-blue quasi-2D perovskite film with improved stability and PLQY, we constructed the PeLEDs with a structure of ITO/PVK (27 nm)/PVP (4 nm)/perovskite (22 nm)/TPBi (40 nm)/LiF (1 nm)/Al (130 nm) [Fig. 4(a)]. The thickness of each layer is further confirmed by the cross-sectional scanning electron microscopy (SEM) image of the device (Fig. S15 in the Supplementary Material). The energy

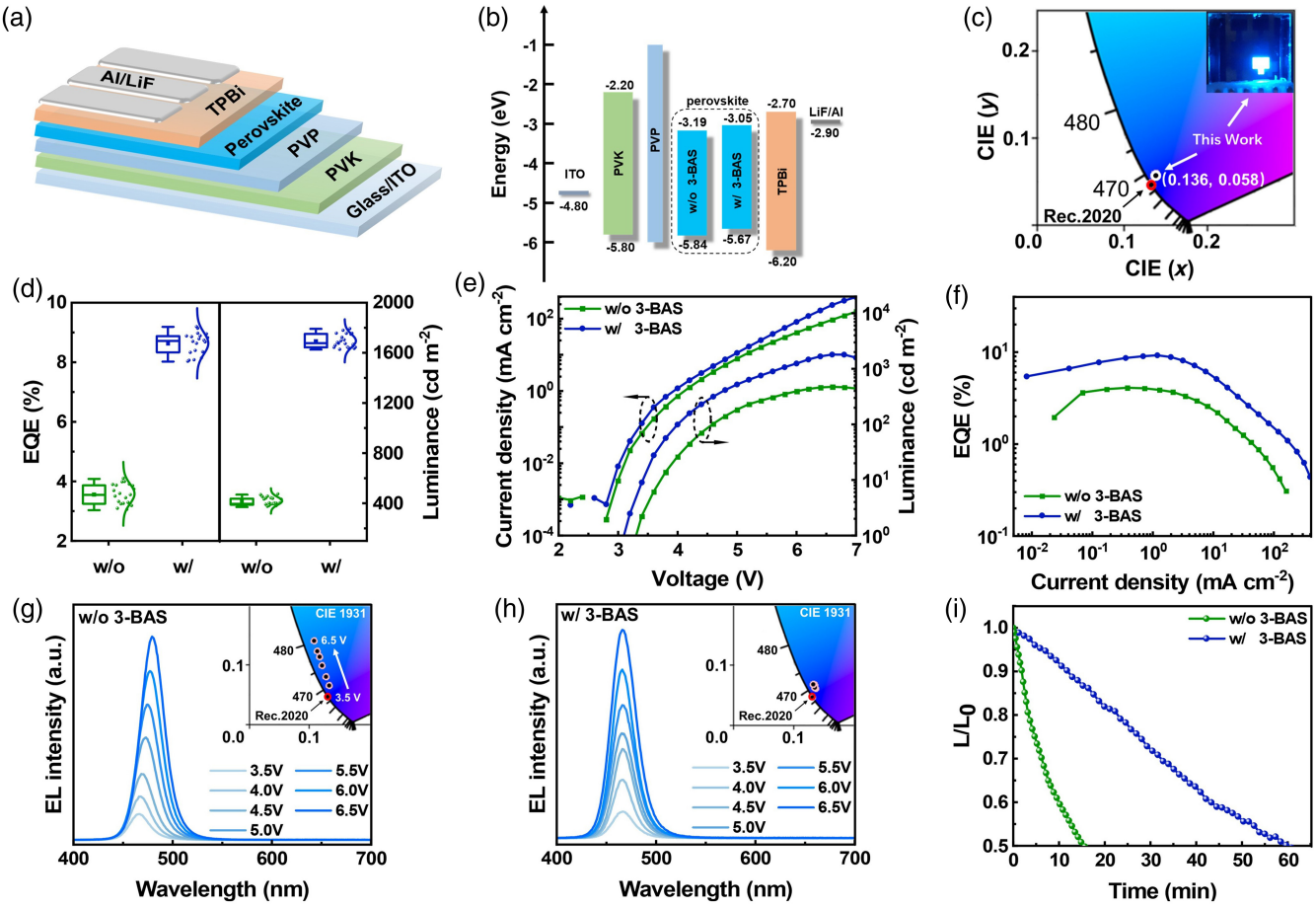

Fig. 4 (a) Device structure. (b) Energy level alignment. (c) Corresponding CIE coordinates of the targeted pure-blue PeLED. The inset shows the photograph of a bright working targeted device at 5 V. (d) Statistical EQEs and luminance of the control and targeted PeLEDs. (e) J-L-V and (f) J-EQE curves. EL stability of the (g) control and (h) targeted PeLEDs with increasing voltage. (i) Operational stability of the control and targeted PeLEDs.

bandgap values of the control and targeted perovskites are calculated by assisting UV photoelectron spectroscopy and optical bandgap estimation. The valence band is estimated to be −5.67 and −5.84 eV for the targeted and control perovskites, respectively (Fig. S16 in the Supplementary Material). The better energy level matching the hole/electron transport layers and the targeted perovskite emitter means that there is a balanced charge injection in PeLED [Fig. 4(b)], and thus the higher device performance can be achieved. The EL spectrum of the targeted PeLEDs exhibits a pure-blue emission at 466 nm with Commission Internationale de l'Eclairage (CIE) coordinates of (0.136, 0.058), which is very near to the Rec. 2020 blue primary color [Fig. 4(c)].[42] The EQE and luminance cartograms of the control and targeted perovskites devices are presented in Fig. 4(d). The average EQE and luminance of targeted PeLEDs are 8.63% and 1696 cd m^{-2}, with a relative standard deviation of 7.2% and 6.5%, respectively, which are much better than the 3.58% and 419 cd m^{-2} of the control perovskites PeLEDs, indicating the good effectiveness and robustness of 3-BAS additive passivation.

Current density–luminance–voltage (J-L-V) and current density-EQE (J-EQE) curves of the champion PeLED are given in Figs. 4(e) and 4(f). It can be seen that the targeted PeLED exhibits a significantly higher current density than that of the control device in the whole voltage operation range [Fig. 4(e)], resulting from the reasonable energy bandgap level in the device and easy charge transfer between individual less-defective perovskite crystals neighboring with delocalized π-electrons on the benzene ring of 3-BAS. Compared with the low peak EQE of 4.1% and the low maximum luminance of 475 cd m^{-2} for the control PeLED, the champion device based on the targeted perovskites exhibits a high peak EQE of 9.25% and a very high maximum luminance of 1806 cd m^{-2}. The influence of different perovskite film thicknesses on device performance was also investigated (Fig. S17 in the Supplementary Material). The results showed that the best device performance was achieved under the perovskite layer thickness of about 20 nm. To the best of our knowledge, these performance parameters situate at the forefront of the literature reporting related experiment results (Table S3 in the Supplementary Material), and especially the maximum luminance is higher than the previous record for pure-blue quasi-2D PeLEDs so far, due to effective defect passivation and efficient energy transfer process by dimensional control. The EL spectrum stability is also evaluated at different bias voltages from 3.5 to 6.5 V. It can be seen that there is a large EL peak redshift with huge color-coordinated variation for the

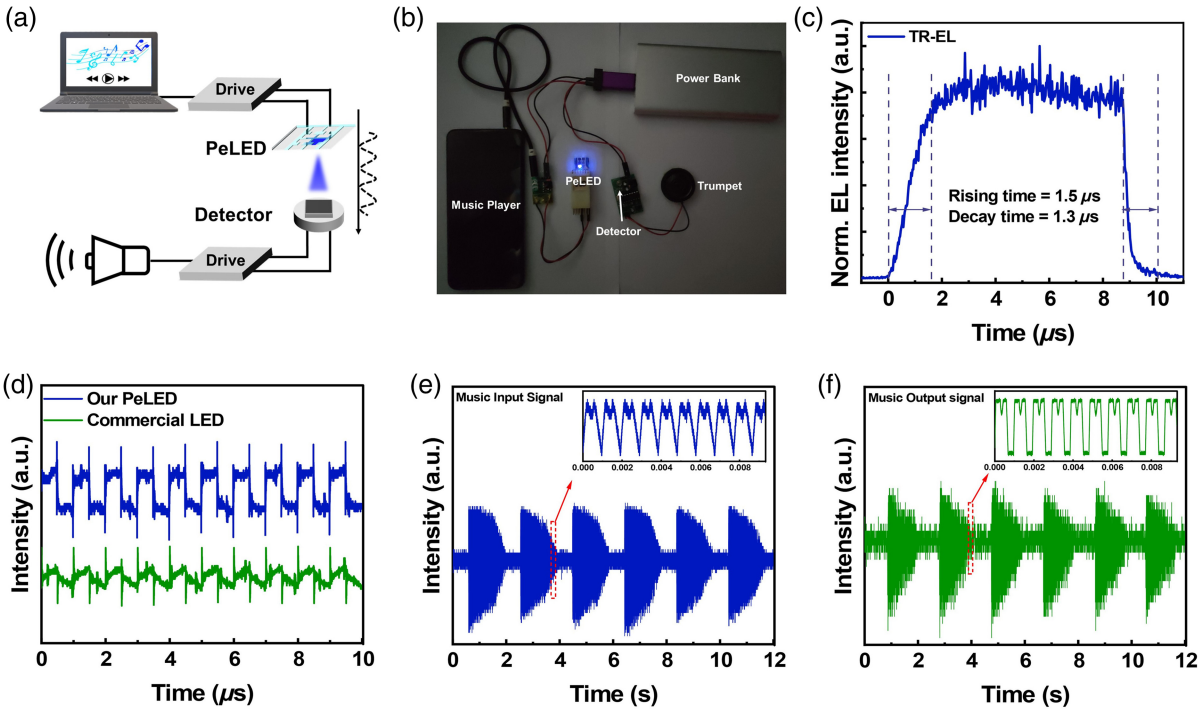

Fig. 5 (a), (b) Schematic and actual experimental setup of the VLC system with the targeted pure-blue PeLED as the light source. (c) Transient EL of the targeted pure-blue PeLED at 3.5 V and 20 kHz with a fixed 20% duty cycle. (d) Square-wave response curves of the targeted pure-blue PeLED and commercial LED at 100 kHz. Comparison of (e) input and (f) output signals in the PeLED-assisted VLC audio transmission system. (Video 1, MP4, 20.7 MB [URL: https://doi.org/10.1117/1.AP.6.2.026002.s1]).

control PeLED [Fig. 4(g)], while the EL spectra of the targeted PeLED remain unchanged at around 466 nm with increasing voltage [Fig. 4(h)]. In addition, we analyzed the color purity trend of PeLEDs under various biases (Fig. S18 in the Supplementary Material). The color purity stability of the targeted device is notably superior to that of the control device, which perfectly matches the color purity requirement for display applications. Furthermore, due to the suppressed halide migration and passivated trap defects in the targeted perovskite film, this device shows a fourfold T_{50} operational lifetime longer than the control device under a constant current density of 5 mA cm^{-2} [Fig. 4(i)], further demonstrating the potential of this innovative method for achieving efficient and stable quasi-2D pure-blue PeLEDs.

The successful realization of stable high-brightness pure-blue PeLEDs can meet the requirements for practical applications well,[43–45] especially for shore-to-sea maritime VLC due to the lowest light attenuation in the blue-green light range.[46–48] To validate its effectiveness, we then used the 3-BAS-treated PeLED as a light source, which is combined with a commercial silicon-based photodetector to construct a low-loss VLC system for transmitting an audio signal. The schematic and actual experimental setup, shown in Figs. 5(a) and 5(b), respectively, consists of an optical signal generation module and an electrical signal revivification module. It can be seen that both rise and decay times of the targeted PeLED are <1.5 μs, indicating that the 3-BAS-treated device is very suitable for the VLC system as a high-speed light source [Fig. 5(c)]. When compared to the commercial inorganic LED, the output of the pure-blue PeLED exhibits better square-wave signal restoration ability under high-frequency (100 kHz) square-wave electric field [Fig. 5(d)], indicating that the 3-BAS-treated PeLED has very good application prospects in the field of optical communication. Furthermore, we found that the output voice signal waveform after experiencing optical modulation and electrical conversion almost exactly matches the waveform of the original input music signal [Figs. 5(e) and 5(f)], realizing the successful conversion of electrical–optical–electrical signal in the whole simulative VLC system (Video 1). The above results demonstrate that high-performance pure-blue PeLEDs with excellent wireless communication capacity can be perfectly achieved by multifunctional zwitterionic passivation engineering.

3 Conclusion

In summary, an effective and reliable approach of crystallization regulation and defect passivation with multifunctional zwitterionic 3-BAS has been demonstrated for achieving highly efficient and stable pure-blue PeLEDs. The trap-mediated nonradiative recombination losses related to undercoordinated Pb^{2+} and halide ion migration are greatly suppressed in the pure-blue mixed-halide quasi-2D perovskites, leading to highly improved luminescence efficiency and operational stability with a peak EQE of 9.25% and a spectrally stable emission at 466 nm. Meanwhile, a recorded maximum luminance value of 1806 cd m^{-2} is obtained in the 3-BAS-treated PeLED, which is successfully used as a quick-response low-loss light source for realizing the audio transmission VLC system. This work

highlights the crucial role for enhancing the performance of the pure-blue mixed halide quasi-2D PeLEDs and provides an avenue for the study of future low-loss optical communication applications.

Code and Data Availability

Data underlying the results presented in this paper may be obtained from the authors upon reasonable request.

Acknowledgments

We acknowledge the support of the National Natural Science Foundation of China (NSFC) (61774077, 12304473, 62175094), the Key Projects of Joint Fund of Basic and Applied Basic Research Fund of Guangdong Province (2019B1515120073, 2019B090921002), the Guangdong Science and Technology Research Foundation (2020A1414010036), the High-End Foreign Experts Project (G20200019046), the Young Talent Support Project of Henan Province (2024HYTP001), and the Opening Project of Key Laboratory of Optoelectronic Chemical Materials and Devices, Ministry of Education, Jianghan University (JDGD-202302).

References

1. Y. K. Wang, "Self-assembled monolayer-based blue perovskite LEDs," *Sci. Adv.* **9**(36), eadh2140 (2023).
2. Y. Q. Sun et al., "Bright and stable perovskite light-emitting diodes in the near-infrared range," *Nature* **615**(7954), 830–835 (2023).
3. H. Wang et al., "*In-situ* growth of low-dimensional perovskite-based insular nanocrystals for highly efficient light emitting diodes," *Light Sci. Appl.* **12**(1), 62 (2023).
4. G. Jang et al., "Rapid crystallization-driven high-efficiency phase-pure deep-blue Ruddlesden-Popper perovskite light-emitting diodes," *Adv. Photonics* **5**(1), 016001 (2023).
5. B. D. Zhao et al., "Light management for perovskite light-emitting diodes," *Nat. Nanotechnol.* **18**(9), 981–992 (2023).
6. Z. K. Tan et al., "Bright light-emitting diodes based on organo-metal halide perovskite," *Nat. Nanotechnol.* **9**(9), 687–692 (2014).
7. J. B. Zhang et al., "A multifunctional 'halide-equivalent' anion enabling efficient $CsPb(Br/I)_3$ nanocrystals pure-red light-emitting diodes with external quantum efficiency exceeding 23%," *Adv. Mater.* **35**(8), 2209002 (2023).
8. J. B. Zhang et al., "Ligand-induced cation-Π interactions enable high-efficiency, bright and spectrally stable Rec. 2020 pure-red perovskite light-emitting diodes," *Adv. Mater.* **35**(45), 2303938 (2023).
9. W. D. Xu et al., "Rational molecular passivation for high-performance perovskite light-emitting diodes," *Nat. Photonics* **13**(6), 418–424 (2019).
10. W. H. Bai et al., "Perovskite light-emitting diodes with an external quantum efficiency exceeding 30%," *Adv. Mater.* **35**(39), 2302283 (2023).
11. Z. M. Chu et al., "Blue light-emitting diodes based on quasi-two-dimensional perovskite with efficient charge injection and optimized phase distribution via an alkali metal salt," *Nat. Electron.* **6**, 360–369 (2023).
12. Y. J. Liu et al., "A multifunctional additive strategy enables efficient pure-blue perovskite light-emitting diodes," *Adv. Mater.* **35**(35), 2302161 (2023).
13. L. Zhang et al., "Manipulating local lattice distortion for spectrally stable and efficient mixed-halide blue perovskite LEDs," *Angew. Chem. Int. Ed.* **62**(21), e202302184 (2023).
14. L. Shu et al., "Highly efficient blue light-emitting diodes based on perovskite film with vertically graded bandgap and organic grain boundary passivation shells," *Adv. Funct. Mater.* **33**(46), 2306570 (2023).
15. S. Yuan et al., "Efficient and spectrally stable blue perovskite light-emitting diodes employing a cationic π-conjugated polymer," *Adv. Mater.* **33**(45), 2103640 (2021).
16. M. Karlsson et al., "Mixed halide perovskites for spectrally stable and high-efficiency blue light-emitting diodes," *Nat. Commun.* **12**(1), 361 (2021).
17. X. F. Liang et al., "Promoting energy transfer between quasi-2D perovskite layers toward highly efficient red light-emitting diodes," *Small* **18**(49), 2204638 (2022).
18. J. B. Zhang et al., "Enhancing stability of red perovskite nanocrystals through copper substitution for efficient light-emitting diodes," *Nano Energy* **62**, 434–441 (2019).
19. Z. Y. Guo et al., "Homogeneous phase distribution in Q-2D perovskites via co-assembly of spacer cations for efficient light-emitting diodes," *Adv. Mater.* **35**(38), 2302711 (2023).
20. S. C. Liu et al., "Zwitterions narrow distribution of perovskite quantum wells for blue light-emitting diodes with efficiency exceeding 15%," *Adv. Mater.* **35**(3), 2208078 (2023).
21. H. W. Zhu et al., "Enriched-bromine surface state for stable sky-blue spectrum perovskite QLEDs with an EQE of 14.6%," *Adv. Mater.* **34**(37), 2205092 (2022).
22. X. Y. Shen et al., "Bright and efficient pure red perovskite nanocrystals light-emitting devices via *in situ* modification," *Adv. Funct. Mater.* **32**(8), 2110048 (2022).
23. K. Datta et al., "Light-induced halide segregation in 2D and quasi-2D mixed-halide perovskites," *ACS Energy Lett.* **8**(4), 1662–1670 (2023).
24. B. Cai et al., "A new descriptor for complicated effects of electronic density of states on ion migration," *Adv. Funct. Mater.* **33**(29), 2300445 (2023).
25. B. B. Guo et al., "Ultrastable near-infrared perovskite light-emitting diodes," *Nat. Photonics* **16**(9), 637–643 (2022).
26. D. X. Ma et al., "Distribution control enables efficient reduced-dimensional perovskite LEDs," *Nature* **599**(7886), 594–598 (2021).
27. A. Walsh, "Principles of chemical bonding and band gap engineering in hybrid organic-inorganic halide perovskites," *J. Phys. Chem. C* **119**(11), 5755–5760 (2015).
28. K. L. Svane et al., "How strong is the hydrogen bond in hybrid perovskites?" *J. Phys. Chem. Lett.* **8**(24), 6154–6159 (2017).
29. J. Zhang et al., "Sulfonic zwitterion for passivating deep and shallow level defects in perovskite light-emitting diodes," *Adv. Funct. Mater.* **32**(22), 2111578 (2022).
30. J. N. Yang et al., "Pseudohalogen resurfaced $CsPbBr_3$ nanocrystals for bright, efficient, and stable green-light-emitting diodes," *Nano Lett.* **23**(8), 3385–3393 (2023).
31. P. Lu et al., "Enrichment of anchoring sites by introducing supramolecular halogen bonds for the efficient perovskite nanocrystal LEDs," *Light Sci. Appl.* **12**(1), 215 (2023).
32. X. J. Gu et al., "Rational surface-defect control via designed passivation for high-efficiency inorganic perovskite solar cells," *Angew. Chem. Int. Ed.* **60**(43), 23164–23170 (2021).
33. H. F. Zhao et al., "High-brightness perovskite light-emitting diodes based on $FAPbBr_3$ nanocrystals with rationally designed aromatic ligands," *ACS Energy Lett.* **6**(7), 2395–2403 (2021).
34. L. M. Kong et al., "Smoothing the energy transfer pathway in quasi-2D perovskite films using methanesulfonate leads to highly efficient light-emitting devices," *Nat. Commun.* **12**(1), 1246 (2021).
35. Y. H. Zhou et al., "Perovskite anion exchange: a microdynamics model and a polar adsorption strategy for precise control of luminescence color," *Adv. Funct. Mater.* **31**(51), 2106871 (2021).
36. L. Y. Wu et al., "Stabilization of inorganic perovskite solar cells with a 2D Dion-Jacobson passivating layer," *Adv. Mater.* **35**(42), 2304150 (2023).

37. C. Li. et al., "Understanding the improvement in the stability of a self-assembled multiple-quantum well perovskite light-emitting diode," *J. Phys. Chem. Lett.* **10**(21), 6857–6864 (2019).
38. A. Q. Liu et al., "Multiple phase regulation enables efficient and bright quasi-2D perovskite light-emitting diodes," *Nano Lett.* **23**(23), 11082–11090 (2023).
39. Y. S. Shin et al., "Manipulated interface for enhanced energy cascade in quasi-2D blue perovskite light-emitting diodes," *ACS Energy Lett.* **7**(10), 3345–3352 (2022).
40. Z. Liu et al., "Deep-red perovskite light-emitting diodes with external quantum efficiency exceeding 21% enabled by ligand-modulated dimensionality control," *Adv. Opt. Mater.* **10**(20), 2201123 (2022).
41. L. M. Kong et al., "A spacer cation assisted nucleation and growth strategy enables efficient and high-luminance quasi-2D perovskite LEDs," *Adv. Funct. Mater.* **33**(2), 2209186 (2022).
42. R. D. Zhu et al., "Realizing Rec. 2020 color gamut with quantum dot displays," *Opt. Express* **23**(18), 23680–23693 (2015).
43. C. X. Bao et al., "Bidirectional optical signal transmission between two identical devices using perovskite diodes," *Nat. Electron.* **3**(3), 156–164 (2020).
44. Q. S. Shan et al., "Perovskite light-emitting/detecting bifunctional fibres for wearable LiFi communication," *Light: Sci. Appl.* **9**(1), 163 (2020).
45. M. L. Xia et al., "Ultrastable perovskite nanocrystals in all-inorganic transparent matrix for high-speed underwater wireless optical communication," *Adv. Opt. Mater.* **9**(12), 2002239 (2021).
46. J. Sticklus et al., "Optical underwater communication: the potential of using converted green LEDs in coastal waters," *IEEE J. Oceanic Eng.* **44**(2), 535–547 (2018).
47. H. M. Oubei et al., "4.8 Gbit/s 16-QAM-OFDM transmission based on compact 450-nm laser for underwater wireless optical communication," *Opt. Express* **23**(18), 23302–23309 (2015).
48. W. Lei et al., "Asymmetric additive-assisted organic solar cells with much better energy harvesting and wireless communication performance," *Adv. Energy Mater.* **13**(40), 2301755 (2023).
49. H. J. Monkhorst and J. D. Pack, "Special points for Brillouin-zone integrations," *Phys. Rev. B* **13**(12), 5188–5192 (1976).
50. J. P. Perdew et al., "Generalized gradient approximation made simple," *Phys. Rev. Lett.* **77**(18), 3865–3868 (1996).
51. G. Kresse and D. Joubert, "From ultrasoft pseudopotentials to the projector augmented-wave method," *Phys. Rev. B* **59**(3), 1758–1775 (1999).
52. N. Yantara et al., "Designing the perovskite structural landscape for efficient blue emission," *ACS Energy Lett.* **5**(5), 1593–1600 (2020).
53. Y. Shen et al., "Interfacial potassium-guided grain growth for efficient deep-blue perovskite light-emitting diodes," *Adv. Funct. Mater.* **31**(6), 2006736 (2021).
54. Y. C. Kim et al., "High-performance perovskite-based blue light-emitting diodes with operational stability by using organic ammonium cations as passivating agents," *Adv. Funct. Mater.* **31**(5), 2005553 (2021).
55. A. Mishra et al., "Leveraging a stable perovskite composite to satisfy blue electroluminescence standards," *ACS Mater. Lett.* **3**(9), 1357–1362 (2021).
56. S. H. Zhao et al., "Postdeposition halide exchange for achieving deep-blue perovskite light-emitting diodes: the role of the organic cations in the chloride source," *Small Methods* **8**, 2300572 (2023).

Chao Shen received his master's degree in electronic information from Jinan University, Guangzhou, China, in 2023. He is currently a PhD candidate in the Department of Optoelectronic Engineering, Jinan University, Guangzhou, China. His research focuses mainly on the metal halide perovskite light-emitting diodes and optical fiber sensing.

Jibin Zhang received his PhD from Huazhong University of Science and Technology in 2020. From 2020 to 2022, he was engaged in postdoctoral research in Jinan University and Linköping University. Then, he was appointed a researcher at Zhengzhou University. His main research interests include metal halide perovskite, perovskite nanocrystals, and their application in photoelectric devices.

Yunhan Luo received his PhD from Tianjin University, Tianjin, China, in 2006. He is currently a professor at Jinan University, Guangzhou, China. His research interests include biomedical photonics, optofluidics, micro/nanophotonics, and optical fiber sensing.

Lintao Hou received his PhD in 2006 from South China University of Technology. He then joined Jinan University as a teacher. From 2009 to 2011, he worked in Linköping University as a postdoc. In 2014, he became a full professor at Jinan University. His research focuses on printed optoelectronic devices and optical simulation.

Biographies of the other authors are not available.